



# 1 **Measurement report: High contribution of N<sub>2</sub>O<sub>5</sub> uptake** 2 **to particulate nitrate formation in NO<sub>2</sub>-limited urban** 3 **areas**

4 Ziyi Lin<sup>1,2,3</sup>, Chuanyou Ying<sup>4</sup>, Lingling Xu<sup>1,2\*</sup>, Xiaoting Ji<sup>1,2,3</sup>, Keran Zhang<sup>1,2</sup>, Feng  
5 Zhang<sup>2</sup>, Gaojie Chen<sup>1,2,3</sup>, Lingjun Li<sup>1,2,3</sup>, Chen Yang<sup>1,2,3</sup>, Yuping Chen<sup>1,2,3</sup>, Ziyang  
6 Chen<sup>1,2,3</sup>, Jinsheng Chen<sup>1,2\*</sup>

## 7 **Affiliations:**

8 <sup>1</sup>State Key Laboratory of Advanced Environmental Technology, Institute of Urban Environment, Chinese  
9 Academy of Sciences, Xiamen 361021, China

10 <sup>2</sup>Fujian Key Laboratory of Atmospheric Ozone Pollution Prevention, Institute of Urban Environment,  
11 Chinese Academy of Sciences, Xiamen 361021, China

12 <sup>3</sup>University of Chinese Academy of Sciences, Beijing 100049, China

13 <sup>4</sup>Fuzhou Institute of Environmental Science, Fuzhou 350013, China

14  
15  
16 *\*Correspondence to:* Jinsheng Chen (jschen@iue.ac.cn); Lingling Xu (linglingxu@iue.ac.cn)  
17

18 **Abstract:** Particulate nitrate (pNO<sub>3</sub><sup>-</sup>) is a major component of fine particle in Chinese urban areas.  
19 However, the relative contributions of pNO<sub>3</sub><sup>-</sup> formation pathways in NO<sub>2</sub>-limited urban areas remain  
20 poorly quantified, hindering further particulate pollution control. In this study, comprehensive winter  
21 field observations were conducted in urban Xiamen, Southeast China. We observed significantly elevated  
22 nighttime pNO<sub>3</sub><sup>-</sup> levels concurrent with increased N<sub>2</sub>O<sub>5</sub> concentrations. Quantification using an  
23 observation-constrained model revealed that N<sub>2</sub>O<sub>5</sub> uptake contributed 51.2% to total pNO<sub>3</sub><sup>-</sup> formation,  
24 which was comparable to that of the OH + NO<sub>2</sub> reaction. The N<sub>2</sub>O<sub>5</sub> uptake was found to be mainly driven  
25 by nocturnal NO<sub>3</sub> oxidation capacity (modulated by NO<sub>2</sub> and O<sub>3</sub> levels) rather than by heterogeneous  
26 reaction conditions. Sensitivity simulations further demonstrated that pNO<sub>3</sub><sup>-</sup> formation rate was more  
27 sensitive to NO<sub>x</sub> variations than to VOCs variations. Implementing NO<sub>x</sub> control measures at nighttime  
28 was shown to effectively reduce pNO<sub>3</sub><sup>-</sup> by abating N<sub>2</sub>O<sub>5</sub> uptake while simultaneously preventing daytime  
29 O<sub>3</sub> increase. Our findings enhance the understanding of pNO<sub>3</sub><sup>-</sup> formation in NO<sub>2</sub>-limited urban areas and  
30 provide valuable insights for developing joint PM<sub>2.5</sub> and O<sub>3</sub> mitigation strategies.

31

32

33



## 1 Introduction

Fine particulate matter (PM<sub>2.5</sub>) contributes to various atmospheric environmental issues, including visibility deterioration, radiative forcing change, and adverse impacts on human health (Seinfeld, 1989; Lelieveld et al., 2015). Among its chemical components, particulate nitrate (pNO<sub>3</sub><sup>-</sup>) has attracted increasing attention due to its rising mass fraction in PM<sub>2.5</sub> and its nonlinear responses to emission mitigation strategies (Xie et al., 2022; Zhai et al., 2021; Li et al., 2021; Zhang et al., 2021; Zhou et al., 2022; Zong et al., 2022; Wang et al., 2020). The primary formation pathways of pNO<sub>3</sub><sup>-</sup> include gas-phase oxidation through the reaction of hydroxyl radicals (OH) and nitrogen dioxides (NO<sub>2</sub>) (R1–R2), and heterogeneous uptake of dinitrogen pentoxide (N<sub>2</sub>O<sub>5</sub>) which is produced via NO<sub>2</sub> oxidation by nitrate radicals (NO<sub>3</sub>) (R3–R5) (Brown and Stutz, 2012). It is well recognized that the OH + NO<sub>2</sub> reaction dominates in daytime, while N<sub>2</sub>O<sub>5</sub> uptake dominates in nighttime. During nocturnal pNO<sub>3</sub><sup>-</sup> formation, particulate chlorides can induce N<sub>2</sub>O<sub>5</sub> heterogeneous uptake to produce ClNO<sub>2</sub>, thereby competing with pNO<sub>3</sub><sup>-</sup> formation.



Many studies have focused on quantifying the potential formation pathways of pNO<sub>3</sub><sup>-</sup> in urban areas of China. In major urban agglomerations such as the Beijing-Tianjin-Hebei (BTH) region (Chen et al., 2020; Ma et al., 2023; Zhao et al., 2023), Yangtze River Delta (YRD) (Sun et al., 2022; Zhai et al., 2023; Zhang et al., 2023b), and Pearl River Delta (PRD) (Yang et al., 2022; Niu et al., 2022; Cheng et al., 2024), pNO<sub>3</sub><sup>-</sup> formation was typically dominated by the gas-phase oxidation of OH + NO<sub>2</sub>. In contrast, under special conditions such as the COVID-19 pandemic and PM<sub>2.5</sub> pollution events (Yan et al., 2023; Zhai et al., 2023), N<sub>2</sub>O<sub>5</sub> uptake became the main pathway. Previous research has demonstrated that the formation rate of pNO<sub>3</sub><sup>-</sup> via N<sub>2</sub>O<sub>5</sub> uptake is closely related to its precursor NO<sub>2</sub> and O<sub>3</sub>, and the N<sub>2</sub>O<sub>5</sub> formation can be classified into NO<sub>2</sub>-limited and O<sub>3</sub>-limited regimes based on the NO<sub>2</sub>/O<sub>3</sub> ratio (Ma et al., 2023). The winter NO<sub>2</sub>/O<sub>3</sub> ratios in the BTH, YRD, and PRD regions were generally above 1, placing N<sub>2</sub>O<sub>5</sub> formation



62 in the  $O_3$ -limited or transition regime (Ma et al., 2023; Wen et al., 2018; Li et al., 2021; Zhang et al.,  
 63 2023b). However,  $N_2O_5$  uptake served as the dominant pathway for  $pNO_3^-$  formation, typically occurring  
 64 under  $NO_2$ -limited conditions (e.g., reduced emissions during the pandemic) or highly favorable  $N_2O_5$   
 65 uptake conditions (e.g., severe particulate pollution episodes). Collectively, these findings indicate that  
 66 spatial variations in  $NO_2$  and  $O_3$  levels are likely a key driver of regional differences in the dominant  
 67 formation pathways of  $pNO_3^-$ . The formation of  $pNO_3^-$  primarily depends on precursors OH,  $NO_2$ , and  
 68  $O_3$ , with OH and  $O_3$  concentrations being influenced by VOCs and  $NO_x$  emissions. Thus, the different  
 69 formation pathways of  $pNO_3^-$  result in complex responses to  $NO_x$ /VOCs emissions. As for the response  
 70 of OH +  $NO_2$  to precursors variation, it was relatively well-understood, as most Chinese urban areas are  
 71 located in VOC-limited regimes for  $O_3$  (Wang et al., 2023b; Wang et al., 2022c; Zhang et al., 2023a; Mao  
 72 et al., 2022), and ammonia-rich regimes for  $pNO_3^-$  (Xing et al., 2018; Sun et al., 2022; Fu et al., 2024;  
 73 Liu et al., 2019). Under these conditions, VOCs reduction suppresses  $pNO_3^-$  formation by decreasing OH  
 74 concentrations, whereas  $NO_x$  reduction enhances  $pNO_3^-$  formation by weakening the  $NO_x$  titration effect.  
 75 Given the regional variations in the  $NO_2/O_3$  ratio across urban areas of China (Ma et al., 2023), the  
 76 response of  $N_2O_5$  uptake to precursor changes (VOCs,  $O_3$ ) likely exhibits spatial heterogeneity. A recent  
 77 study has revealed that under  $O_3$ -limited conditions for  $N_2O_5$  formation (Zhang et al., 2023b),  $NO_x$   
 78 emissions had negligible effects, while VOCs reduction decreased the removal of  $NO_3$  by VOCs, thereby  
 79 enhancing  $N_2O_5$  uptake. However, the response of  $pNO_3^-$  formation to precursors under  $NO_2$ -limited  
 80 conditions remains unclear. Aside from precursor availability,  $N_2O_5$  uptake is also greatly influenced by  
 81 heterogeneous reaction conditions like aerosol composition and aerosol surface area (McDuffie et al.,  
 82 2018b; McDuffie et al., 2018a; Tham et al., 2018; Yu et al., 2020), which introduces additional uncertainty  
 83 in determining the contribution of  $pNO_3^-$  formation pathways and the effectiveness of precursor control  
 84 strategies.

85 The  $NO_2/O_3$  ratios in southeastern China predominantly fell within the  $NO_2$ -limited regime for  $N_2O_5$   
 86 formation (Ma et al., 2023). Xiamen, as one of the most developed cities in southeastern China, exhibits  
 87 relatively better air quality with low levels of VOCs and  $NO_x$  compared to China's megacities (**Table**  
 88 **S1**). This pattern well represents the future urban atmospheric conditions following the implementation  
 89 of air pollution control measures in China. From December 2022 to February 2023, we conducted  
 90 comprehensive multi-parameter observations in urban Xiamen, including  $N_2O_5$  and related chemical  
 91 constituents. An observation-constrained box model incorporating the heterogeneous reaction parameters



was utilized to quantify the rates of different  $\text{pNO}_3^-$  formation pathways. Explainable machine learning (ML) method was applied to identify the driving factors of high  $\text{N}_2\text{O}_5$  uptake rate. Additionally, multi-scenario simulations were performed to examine the joint responses of  $\text{pNO}_3^-$  and  $\text{O}_3$  formation to various  $\text{NO}_x$  and VOCs emissions. These findings enhance our understanding of  $\text{pNO}_3^-$  formation pathways and their environmental implications in  $\text{NO}_2$ -limited regions, providing valuable insights for developing joint  $\text{PM}_{2.5}$  and  $\text{O}_3$  mitigation strategies.

## 2 Methods

### 2.1 Field Observation.

Field observations were conducted during the winter period from 1 December 2022 to 3 February 2023, at an urban site (marked by the red star in **Figure S1**) in Xiamen, which is located in the southeastern coastal region of China. Detailed site information has been described in our previous studies (Yang et al., 2023; Liu et al., 2022). Trace gases (including PAN, HCHO, HONO, VOCs,  $\text{O}_3$ ,  $\text{NO}_x$ , CO, and  $\text{SO}_2$ ), chemical components in  $\text{PM}_{2.5}$  (including organic carbon and elemental carbon,  $\text{SO}_4^{2-}$ ,  $\text{NO}_3^-$ ,  $\text{NH}_4^+$ ,  $\text{Cl}^-$ ),  $\text{PM}_{2.5}$  mass concentration, and meteorological parameters (including ambient temperature (T), relative humidity (RH), atmospheric pressure (P), wind speed (WS), wind direction (WD), and photolysis rates) were continuously measured during the campaign. Detailed information about measurement methods and instruments is summarized in **Text S1**. A chemical ionization time-of-flight mass spectrometer equipped with an iodide source (iodide-TOF-CIMS, Aerodyne Research Inc., USA) was deployed to measure  $\text{N}_2\text{O}_5$  and  $\text{ClNO}_2$ . The instrument configuration and calibration procedures for  $\text{N}_2\text{O}_5$  and  $\text{ClNO}_2$  are described in **Text S2**, following established methods (Wang et al., 2022b; Wang et al., 2022a; Thaler et al., 2011). Boundary layer height (BLH) data were obtained from the ERA5 dataset (Hersbach et al., 2020).

### 2.2 Determination of $\text{pNO}_3^-$ Formation Rate.

The interactive box model developed by Wagner et al. with a simplified mechanism was employed to obtain key parameters of the  $\text{N}_2\text{O}_5$  uptake process (Wagner et al., 2013), including  $k\text{N}_2\text{O}_5$  and  $\phi\text{ClNO}_2$  (see in **Text S3**). To validate the interactive box model results, these parameters were calculated concurrently based on the classical steady-state approximation method (**Text S4**) (Brown et al., 2003; Chen et al., 2022). As shown in **Figure S2**, the outcomes of the two methods exhibited strong consistency, with logarithmic correlation coefficients ( $R^2$ ) as high as 0.76 and 0.73 for  $k\text{N}_2\text{O}_5$ ,  $\phi\text{ClNO}_2$ , respectively.



122 Considering the larger number of valid data points, the model-derived parameters were adopted for  
 123 subsequent analysis.

124 A Framework for 0-D Atmospheric Modeling (F0AM), incorporating the Master Chemical  
 125 Mechanism (MCM v3.3.1) and heterogeneous mechanisms (**Table S2**), was employed to simulate nitrate  
 126 formation rates for each day during the study period (Wolfe et al., 2016; Atkinson and Arey, 2003; Jenkin  
 127 et al., 2015). The heterogeneous parameters derived from the interactive box model were implemented  
 128 in F0AM. In addition, hourly interval data of trace gases, photochemically active species, meteorological  
 129 variables, and reanalysis data were also applied to constrain the multiphase chemical box model. Detailed  
 130 model configurations are provided in **Text S5**. As shown in **Figure S3**, the model performed well for  
 131  $\text{N}_2\text{O}_5$  and  $\text{ClNO}_2$  simulations with  $R^2$  of 0.88 and 0.49, respectively. The simulated OH concentrations  
 132 agreed well with parameterized method suggested by Ehhalt and Rohrer (**Figure S4**,  $R^2 = 0.86$ ) (Ehhalt  
 133 and Rohrer, 2000). Based on model simulation and precursor observations, we quantified  $\text{pNO}_3^-$   
 134 formation rates through both  $\text{OH} + \text{NO}_2$  and  $\text{N}_2\text{O}_5$  uptake pathways by model integral. Note that the gas-  
 135 particle partitioning coefficient was set to 100%, which might lead to an overestimation of the  $\text{OH} +$   
 136  $\text{NO}_2$  pathway contribution.

137

### 138 **2.3 Identification of influencing factors for $\text{N}_2\text{O}_5$ uptake.**

139 Extreme gradient boosting (XGBoost), a machine learning technique, has been widely applied in  
 140 atmospheric chemistry research (Gui et al., 2020; Wang et al., 2023c; Requia et al., 2020). Here, we built  
 141 a XGBoost model to reproduce the  $\text{N}_2\text{O}_5$  uptake rate with selected variables. The model was built using  
 142 the “xgboost” library (<https://github.com/dmlc/xgboost/tree/master>) in a python environment.  
 143 Explanatory variables included meteorological parameters (BLH, T, and RH), nocturnal atmospheric  
 144 oxidation capacity  $\text{P}(\text{NO}_3)$  calculated by  $k_{\text{NO}_2+\text{O}_3}[\text{NO}_2][\text{O}_3]$ , TVOCs, the logarithm of the ratio of  $\text{NO}_2$   
 145 to  $\text{O}_3$  ( $\log([\text{NO}_2]/[\text{O}_3])$ ), NO, and heterogeneous uptake parameters ( $\phi\text{ClNO}_2$  and  $k\text{N}_2\text{O}_5$ ). Only nighttime  
 146 (18:00 – 06:00 the next day) data were considered to identify key drivers of  $\text{N}_2\text{O}_5$  uptake. The  
 147 hyperparameters of the XGBoost model were tuned by grid searching method and the established model  
 148 was evaluated using  $R^2$ , Mean Absolute Error (MAE) and Root Mean Square Error (RMSE). By  
 149 incorporating SHAP interpretation, the XGBoost-SHAP method could quantify factor contributions  
 150 through SHAP values, where absolute SHAP values denote the relative importance. Detailed description  
 151 and setup of the XGBoost-SHAP method can be found in **Text S6** and our previous study (Lin et al.,



2024).

## 2.4 Emission Scenario Modelling.

Using the aforementioned multiphase chemical box model, we investigated changes in formation rates of  $\text{pNO}_3^-$  ( $\text{PNO}_3^-$ ) and  $\text{O}_3$  ( $\text{PO}_3$ ) under different VOCs and  $\text{NO}_x$  emission scenarios. The base model simulation was performed using mean diurnal values from the winter 2022 observations. A series of emission scenarios were tested by scaling normalized VOCs and  $\text{NO}_x$  concentrations from 0 to 2 times baseline levels to examine their impacts on  $\text{PNO}_3^-$  and  $\text{PO}_3$ . Prior to each scenario simulation, 3-day spin-up was set to stabilize intermediate species concentrations. Isopleth diagrams of simulated  $\text{PNO}_3^-$  and  $\text{PO}_3$  were obtained from the base scenario and 120 emission change scenarios. In addition, response strength (RS) was calculated using **eq 2** as an indicator of emission sensitivity.

$$\text{PO}_3 = k_1[\text{HO}_2][\text{NO}] + \sum k_{2i}[\text{RO}_2][\text{NO}] \quad (1)$$

Where,  $k_i$  is the corresponding chemical reaction rate constants.

$$\text{RS} = \frac{X_i - X_{\text{base}}}{V_i - V_{\text{base}}} \quad (2)$$

Where,  $X_i$  and  $X_{\text{base}}$  are the mean formation rates of dependent variables e.g.  $\text{PNO}_3^-$ ,  $\text{PO}_3$  in scenario  $i$  and base simulations, respectively.  $V_i$  and  $V_{\text{base}}$  are the emission rates for the scenario  $i$  and base simulations, respectively. Notably, the emission rates ranged from 0 to 2 times baseline levels, with the base simulation emission rate normalized to 1.

## 3 Results and Discussion

### 3.1 Overview of Observations.

The mean diurnal patterns of  $\text{pNO}_3^-$ , gaseous pollutants and relevant meteorological parameters are shown in **Figure 1**. During the entire observation period, mean concentrations of  $\text{NO}_2$ ,  $\text{O}_3$ , total VOCs, and  $\text{PM}_{2.5}$  were 10.9 ppb, 27.3 ppb, 18.2 ppb, and  $14.3 \mu\text{g m}^{-3}$ , respectively, lower than those observed in most of China's key cities (refer to **Table S1**). Despite the low  $\text{NO}_x$  levels,  $\text{pNO}_3^-$  contributed 29.5% to  $\text{PM}_{2.5}$  mass concentration, which was higher than proportions reported in Beijing urban area (24.7%) (Ma et al., 2023), Guangdong (24.0%) (Yun et al., 2018), and Nanjing (24%–27%) (Huang et al., 2020). This discrepancy suggests efficient conversion from  $\text{NO}_2$  to  $\text{pNO}_3^-$  in the study area. In addition, the proportion of  $\text{pNO}_3^-$  increased with rising  $\text{PM}_{2.5}$  concentration (**Figure S6**), indicating its importance to



181 particulate pollution. This is consistent with the phenomenon widespread in urban areas of China where  
 182  $\text{pNO}_3^-$  became dominant in inorganic aerosols despite  $\text{NO}_x$  reduction, underscoring the need for efficient  
 183  $\text{pNO}_3^-$  control strategies (Zhai et al., 2021; Zhao et al., 2020; Zhang et al., 2022).

184 The diurnal pattern of  $\text{pNO}_3^-$  exhibited a bimodal characteristic, with peaks occurring at 4:00 and  
 185 16:00 LT, respectively. The daytime peak (07:00–17:00) was accompanied by low concentrations of  $\text{NO}_x$   
 186 and high levels of  $\text{O}_3$  and  $\text{JNO}_2$ , indicating that active photochemical conditions promoted daytime  $\text{pNO}_3^-$   
 187 formation. During the nighttime (18:00–06:00 the next day),  $\text{pNO}_3^-$  concentrations increased together  
 188 with  $\text{NO}_2$ ,  $\text{N}_2\text{O}_5$  and  $\text{ClNO}_2$  from 18:00 onward and remained elevated until early morning. This  
 189 nighttime accumulation can be attributed to two factors. First, lower temperature, shallower boundary  
 190 layer height, and reduced wind speed at night favored the accumulation of  $\text{pNO}_3^-$  and related nitrogen-  
 191 containing species. Second, higher RH and  $\text{PM}_{2.5}$  concentrations at night enhanced aerosol water content  
 192 and surface area, providing favorable conditions for heterogeneous hydrolysis of  $\text{N}_2\text{O}_5$  to form  $\text{pNO}_3^-$ .  
 193 The mean concentration of  $\text{N}_2\text{O}_5$  was  $0.19 \pm 0.26$  ppb (peaking at 2.52 ppb), which is relatively higher  
 194 than values reported for China's megacities (Chen et al., 2020; Wang et al., 2017; Tham et al., 2018;  
 195 Wang et al., 2022a; Liu et al., 2025; Li et al., 2023). Moreover, the observed elevation in nighttime  $\text{ClNO}_2$ ,  
 196 primarily produce via the reaction of  $\text{N}_2\text{O}_5$  with Cl-containing particles, strongly supports the presence  
 197 of active heterogeneous processes of  $\text{N}_2\text{O}_5$ . Collectively, these findings imply a likely significant  
 198 contribution of  $\text{N}_2\text{O}_5$  uptake to  $\text{pNO}_3^-$  formation during the nighttime.

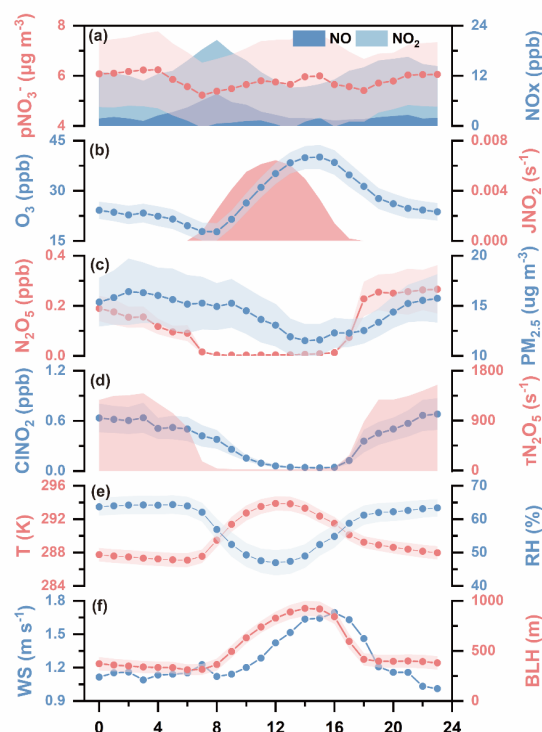


**Figure 1.** Diurnal variations of key parameters during the winter of 2022. The concentrations of  $\text{pNO}_3^-$ ,  $\text{NO}_x$ ,  $\text{O}_3$ ,  $\text{N}_2\text{O}_5$ ,  $\text{PM}_{2.5}$  and  $\text{ClNO}_2$ . The levels of the photolysis frequencies of  $\text{NO}_2$  ( $\text{JNO}_2$ ), ambient temperature ( $T$ ), relative humidity ( $\text{RH}$ ), the lifetime of  $\text{N}_2\text{O}_5$  ( $\tau\text{N}_2\text{O}_5$ ), wind speed ( $\text{WS}$ ) and the boundary layer height ( $\text{BLH}$ ). Shaded areas of  $\text{pNO}_3^-$ ,  $\text{O}_3$ ,  $\text{N}_2\text{O}_5$ ,  $\text{PM}_{2.5}$ ,  $\text{ClNO}_2$ ,  $T$ ,  $\text{RH}$  and  $\text{BLH}$  represent 95% confidence intervals.

### 3.2 High contribution of $\text{N}_2\text{O}_5$ uptake to $\text{pNO}_3^-$ formation in $\text{NO}_2$ -limited conditions.

In view of the observed importance of daytime and nighttime  $\text{pNO}_3^-$  formation, we further employed an observation-constrained model to quantify the potential formation pathways, including the gas-phase reaction of  $\text{OH} + \text{NO}_2$  and heterogeneous  $\text{N}_2\text{O}_5$  uptake. This model incorporated heterogeneous chemical mechanisms, with key heterogeneous parameters (e.g. the loss rate of  $\text{N}_2\text{O}_5$  ( $k\text{N}_2\text{O}_5$ ) and the production yield of  $\text{ClNO}_2$  ( $\phi\text{ClNO}_2$ )) obtained through simulation (See Methods for details). As shown in **Figure S7**, these simulated parameters exhibited good agreement with classical steady-state methods, demonstrating the model's capability to characterize heterogeneous uptake processes and thereby





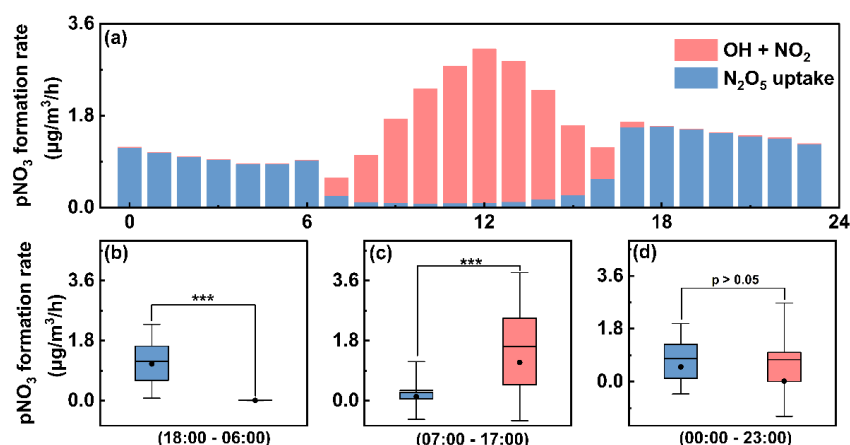
effectively evaluate  $\text{pNO}_3^-$  formation processes.

As illustrated in **Figure 2a**, the diurnal pattern of  $\text{pNO}_3^-$  formation rates exhibited a classical characteristic, with daytime dominated by gas-phase oxidation and nighttime dominated by  $\text{N}_2\text{O}_5$  uptake. The daytime  $\text{OH} + \text{NO}_2$  reaction had a mean  $\text{pNO}_3^-$  formation rate of  $1.62 \mu\text{g m}^{-3} \text{h}^{-1}$ , while the nighttime  $\text{N}_2\text{O}_5$  uptake pathway showed a formation rate of  $1.18 \mu\text{g m}^{-3} \text{h}^{-1}$  (**Figure 2b-c**). For the whole day,  $\text{N}_2\text{O}_5$  uptake contributed an average of 51.2% to  $\text{pNO}_3^-$  formation, which was comparable to the contribution of the  $\text{OH} + \text{NO}_2$  pathway (**Figure 2d**). Notably, the partitioning coefficient for gas-phase oxidation processes was assumed to be 1 in this study, meaning the contribution of  $\text{OH} + \text{NO}_2$  represented an upper limit and the actual contribution of  $\text{N}_2\text{O}_5$  uptake should be even greater. To exclude year-specific effects, we further analyzed the contributions of both pathways to  $\text{pNO}_3^-$  formation during winters from 2019 to 2023. The results demonstrated that  $\text{N}_2\text{O}_5$  uptake pathway consistently accounted for approximately half of  $\text{pNO}_3^-$  formation in the study area (**Figure 3a**), which was also consistent with the observed high proportion of nighttime  $\text{pNO}_3^-$  throughout the day (**Figure 3b**). Such a high contribution of  $\text{N}_2\text{O}_5$  uptake to  $\text{pNO}_3^-$  is generally uncommon in urban areas. A study in urban Beijing showed that during non-polluted periods,  $\text{N}_2\text{O}_5$  uptake contributed only 18.9% to nitrate formation rates (Ma et al., 2023). Similarly, the contributions of  $\text{N}_2\text{O}_5$  uptake were 10%–38% and 4% in urban areas of the YRD (Sun et al., 2022; Zhai et al., 2023; Zhang et al., 2023b) and PRD regions (Yang et al., 2022), respectively.

Previous studies have found that nocturnal  $\text{pNO}_3^-$  formation via  $\text{N}_2\text{O}_5$  uptake strongly depends on the ratio of  $\text{NO}_2$  to  $\text{O}_3$  (Ma et al., 2023). This process is suppressed in the  $\text{O}_3$ -limited regime ( $\text{NO}_2/\text{O}_3 > 2$ ) but enhanced in the  $\text{NO}_2$ -limited regime ( $\text{NO}_2/\text{O}_3 \leq 1$ ). The COVID-19 lockdown period was a typical example of this ratio dependence (Yan et al., 2023). In regions like Beijing, substantial reductions in  $\text{NO}_x$  emissions caused a shift in nocturnal  $\text{pNO}_3^-$  formation from the  $\text{O}_3$ -limited to the  $\text{NO}_2$ -limited regime. This shift resulted in elevated nighttime  $\text{O}_3$  levels and a weakened  $\text{NO}$  titration effect, collectively promoting  $\text{N}_2\text{O}_5$  formation and subsequent  $\text{pNO}_3^-$  formation. The sensitivity of  $\text{N}_2\text{O}_5$  uptake to  $\text{NO}_2$  and  $\text{O}_3$  during the campaign is presented in **Figure 3c-d**. The observed mean values of  $\text{NO}_2/\text{O}_3$  (0.40) and the probability distributions of  $\text{NO}_2/\text{O}_3$  ratios both indicate that  $\text{N}_2\text{O}_5$  uptake was in the  $\text{NO}_2$ -limited regime. Based on  $\text{NO}_2$  and  $\text{O}_3$  observational data during 2015–2021 from the China National Environmental Monitoring Centre (Ma et al., 2023), most key urban regions in China (e.g., the NCP, YRD, and Beijing) were found to lie in the  $\text{O}_3$ -limited or transition regimes ( $1 < \text{NO}_2/\text{O}_3 \leq 2$ ), whereas nocturnal  $\text{pNO}_3^-$  formation in southeastern China was distinctly in  $\text{NO}_2$ -limited regime. These results confirm that the dominant



244  $\text{pNO}_3^-$  formation mechanisms in our study area significantly differs from those in most urban areas of  
 245 China, which might be attributed to the dependence of  $\text{N}_2\text{O}_5$  uptake on precursor  $\text{NO}_2$  and  $\text{O}_3$ . In addition,  
 246 the dominance of  $\text{N}_2\text{O}_5$  uptake in  $\text{pNO}_3^-$  formation also occurred during haze pollution periods (Zhai et  
 247 al., 2023; Wang et al., 2017), where increased aerosol surface area under high particulate loadings created  
 248 favorable conditions for  $\text{N}_2\text{O}_5$  heterogeneous reactions. Therefore, to evaluate the role of precursors, we  
 249 conducted a comprehensive analysis of the factors driving  $\text{pNO}_3^-$  formation via  $\text{N}_2\text{O}_5$  uptake.  
 250



251  
 252 **Figure 2.** Simulated rates of key  $\text{pNO}_3^-$  formation pathways obtained from the chemical box model  
 253 incorporating heterogeneous parameters. Diurnal formation rates of  $\text{pNO}_3^-$  via the  $\text{OH} + \text{NO}_2$  and  $\text{N}_2\text{O}_5$   
 254 uptake pathways (a) and comparison of the two pathways during the nighttime (b), daytime (c), and the  
 255 whole day (d). Note that the results in panel (a) represent the mean simulated formation rates over the  
 256 entire observation period. The box shows the 25th–75th percentiles with whiskers representing the 5th–  
 257 95th percentiles. The black line and dot inside the box represent the mean and median values, respectively.  
 258 Statistical significance was determined using pair-sample  $t$ -tests with \*\*\* indicating  $p < 0.001$ .  
 259

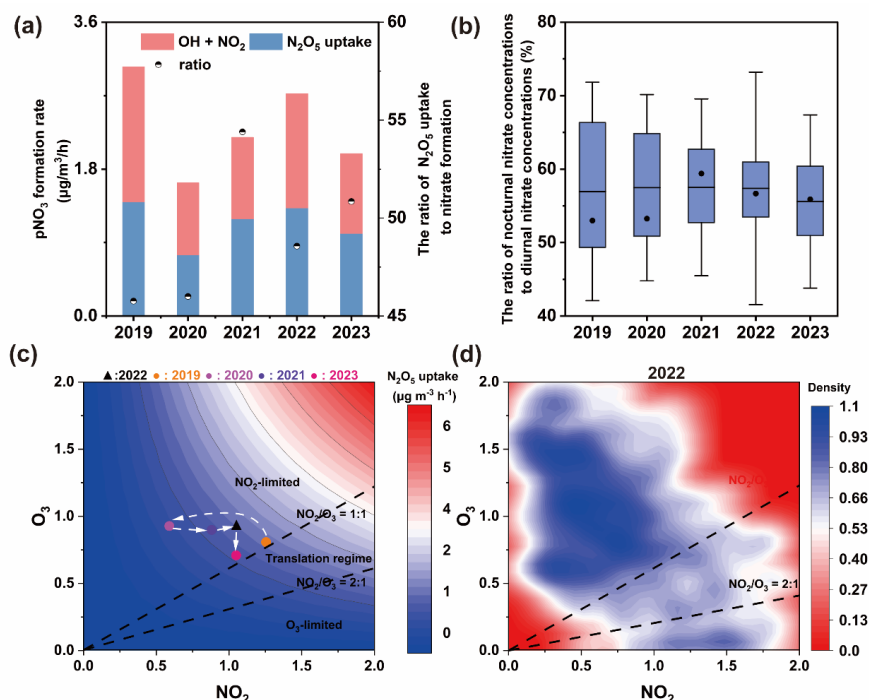


**Figure 3.** Inter-annual patterns of key  $\text{pNO}_3^-$  formation pathways in urban Xiamen. The average  $\text{pNO}_3^-$  formation rate from  $\text{OH} + \text{NO}_2$  and  $\text{N}_2\text{O}_5$  uptake (a), and the average ratio of the sum of nocturnal  $\text{pNO}_3^-$  concentrations to the sum of all-day  $\text{pNO}_3^-$  concentration (b) in different winters from 2019 to 2023 based on the measured  $\text{pNO}_3^-$  in  $\text{PM}_{2.5}$ . The sensitivity of nocturnal  $\text{N}_2\text{O}_5$  uptake to  $\text{NO}_2$  and  $\text{O}_3$  from 2019 to 2023 (c). And probability distribution of observed  $\text{NO}_2/\text{O}_3$  at nighttime in winter 2022 (d). The observed periods of different winters from 2019 to 2023 are summarized in Table S3. In panel (c), the black triangle indicates the base case of winter 2022, solid circles in different colors represent the average  $\text{NO}_2$  to  $\text{O}_3$  ratios in different years, and the predicted average formation rate of  $\text{N}_2\text{O}_5$  uptake as the normalized emissions (average concentrations of  $\text{O}_3$  and  $\text{NO}_2$ ) varied between 0 to 2.

### 3.3 Driving Factors of Nocturnal $\text{N}_2\text{O}_5$ Uptake.

The  $\text{N}_2\text{O}_5$  uptake rate is influenced by multiple factors including precursor levels, meteorological parameters, and heterogeneous reaction conditions (Ma et al., 2023; Chen et al., 2020; Chen et al., 2024). A machine learning method integrating these factors was employed to identify the key drivers of  $\text{N}_2\text{O}_5$  uptake. The relative importance of each factor was evaluated by absolute SHAP values (Figure 4a), and



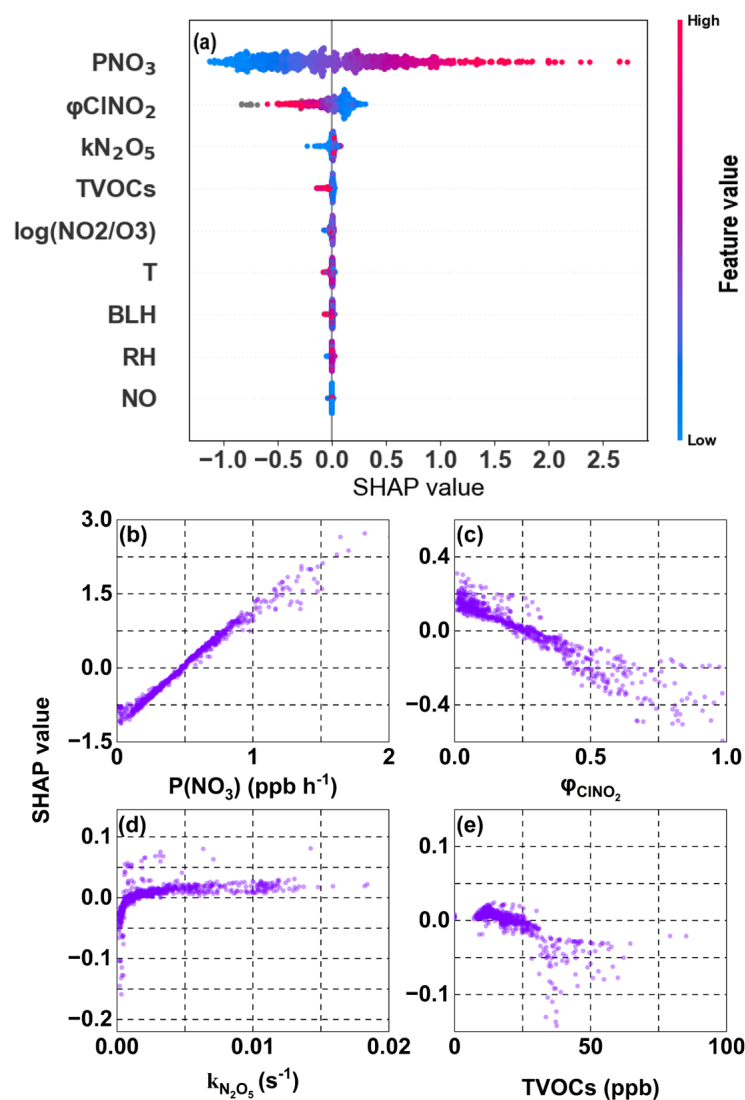
their impacts were elucidated by examining the relationships between individual factors and their corresponding SHAP values (**Figure 4b-e** and **Figure S8**). Results showed that the nocturnal  $\text{NO}_3$  formation rate ( $\text{P}(\text{NO}_3)$ ), an integrated indicator of nocturnal atmospheric oxidation capacity (Wang et al., 2021), was the most important factor for  $\text{N}_2\text{O}_5$  uptake with the highest absolute SHAP value. The steep slope of the positive correlation between  $\text{P}(\text{NO}_3)$  and SHAP values indicated that  $\text{P}(\text{NO}_3)$  strongly enhanced  $\text{N}_2\text{O}_5$  uptake.  $\text{P}(\text{NO}_3)$  is primarily formed through the reaction between  $\text{NO}_2$  and  $\text{O}_3$  ( $\text{P}(\text{NO}_3) = k_{\text{NO}_2+\text{O}_3}[\text{NO}_2][\text{O}_3]$ ), suggesting that  $\text{NO}_2$  and  $\text{O}_3$  mainly influenced  $\text{N}_2\text{O}_5$  uptake by modulating  $\text{NO}_3$  radical formation. Notably, the factor  $\log\text{NO}_2/\text{O}_3$  had relatively low importance, indicating concentrations of precursors were more important than  $\text{NO}_2/\text{O}_3$  ratio in determining the  $\text{N}_2\text{O}_5$  uptake under extremely  $\text{NO}_2$ -limited condition (mean  $\text{NO}_2/\text{O}_3$  was 0.40). Furthermore, as shown in **Figure S8b**,  $\log\text{NO}_2/\text{O}_3$  and its SHAP value shows a positive correlation when  $\log\text{NO}_2/\text{O}_3$  is less than 0. Under  $\text{NO}_2$ -limited conditions ( $\log\text{NO}_2/\text{O}_3 < 0$ ,  $\text{NO}_2/\text{O}_3 < 1$ ),  $\text{N}_2\text{O}_5$  uptake was driven by the elevated  $\text{NO}_2$ .

Compared with  $\text{P}(\text{NO}_3)$ , other factors exhibited weaker effects on  $\text{N}_2\text{O}_5$  uptake.  $\phi\text{ClNO}_2$  emerged as the second most important factor and showed a negative correlation with SHAP values (**Figure 4c**), illustrating that  $\text{ClNO}_2$  formation inhibited  $\text{pNO}_3^-$  formation. This inhibitory effect could be attributed to high concentrations of Cl-containing particles ( $0.94 \pm 1.11 \mu\text{g m}^{-3}$ ) in the study area. Chloride-containing aerosols promote  $\text{N}_2\text{O}_5$  uptake to produce more  $\text{ClNO}_2$  (as evidenced by the positive correlation between  $\phi\text{ClNO}_2$  and chloride ions, **Figure S9**), while simultaneously reducing  $\text{pNO}_3^-$  formation (R5). Additionally, the nighttime produced  $\text{ClNO}_2$  can undergo photolysis in following day to release Cl radicals, which further promote  $\text{O}_3$  formation. This indirect effect must be considered when formulating control measures for particulate matter pollution. Interestingly, as shown in **Table S4** (Tham et al., 2016; Wang et al., 2018; Yun et al., 2018; Morgan et al., 2015), although the simulated  $k_{\text{N}_2\text{O}_5}$  ( $7.64 \times 10^{-3} \pm 6.12 \times 10^{-3} \text{ s}^{-1}$ ) was higher than values reported in Beijing ( $8.1 \times 10^{-4} - 1.42 \times 10^{-3} \text{ s}^{-1}$ ), Guangdong ( $3.78 \times 10^{-3} - 9 \times 10^{-3} \text{ s}^{-1}$ ), and UK ( $9.3 \times 10^{-5} - 10^{-3} \text{ s}^{-1}$ ),  $k_{\text{N}_2\text{O}_5}$  exerted only a weak positive effect on  $\text{N}_2\text{O}_5$  uptake (**Figure 4d**). The large difference existing in importance of  $\text{P}(\text{NO}_3)$  and  $k_{\text{N}_2\text{O}_5}$  indicated that the  $\text{N}_2\text{O}_5$  uptake process was more limited by precursor levels rather than heterogeneous uptake conditions. Similar phenomenon was also found in winter in urban Beijing and Northern Utah mountain basins (Mcduffie et al., 2019; Chen et al., 2020). This situation is likely due to the favorable  $\text{N}_2\text{O}_5$  uptake conditions during winter, e.g., low temperature, high aerosol surface area, and elevated aerosol liquid content (Wang et al., 2023a; Mcduffie et al., 2018b; Jia et al., 2020). The total concentrations of the observed VOCs (TVOCs)



306 showed a weak negative correlation with  $\text{N}_2\text{O}_5$  uptake (**Figure 4e**), reflecting their indirect inhibition on  
307  $\text{N}_2\text{O}_5$  formation by consuming  $\text{NO}_3$  radicals. Moreover, we found that the effects of  $\phi\text{ClNO}_2$ ,  $\text{kN}_2\text{O}_5$ , and  
308 TVOCs on  $\text{N}_2\text{O}_5$  uptake were subject to  $\text{P}(\text{NO}_3)$  levels (**Figure 5a-5c**). Specifically, the negative effect  
309 of  $\phi\text{ClNO}_2$  and the positive effect of  $\text{kN}_2\text{O}_5$  on  $\text{N}_2\text{O}_5$  uptake became statistically significant when  $\text{P}(\text{NO}_3)$   
310 exceeded approximately  $1.0 \text{ ppb h}^{-1}$  and  $0.5 \text{ ppb h}^{-1}$ , respectively. The negative correlation slope of  
311 TVOCs versus  $\text{N}_2\text{O}_5$  uptake intensified with increasing  $\text{P}(\text{NO}_3)$  levels, indicating that the  $\text{N}_2\text{O}_5$  removal  
312 effect was enhanced through VOC-induced  $\text{NO}_3$  depletion. These findings highlight the critical role of  
313 precursor  $\text{NO}_2$  and  $\text{O}_3$  in nocturnal  $\text{pNO}_3^-$  formation, demonstrating that these precursors mainly affect  
314 this pathway by modulating  $\text{NO}_3$  radical formation.

315



316  
 317 **Figure 4.** Feature importance (a) and the effects of key factors on  $N_2O_5$  uptake (b-e) obtained by the  
 318 XGBoost-SHAP method. The relationships between SHAP values and major features:  $P(NO_3)$  (b),  
 319  $\phi CINO_2$ (c),  $k_{N_2O_5}$ (d), and TVOCs (e). Feature importance ranking (a) is determined by mean absolute  
 320 SHAP values (descending order, top to bottom). Relationships between SHAP values and other factors  
 321 are shown in **Figure S8**.  
 322

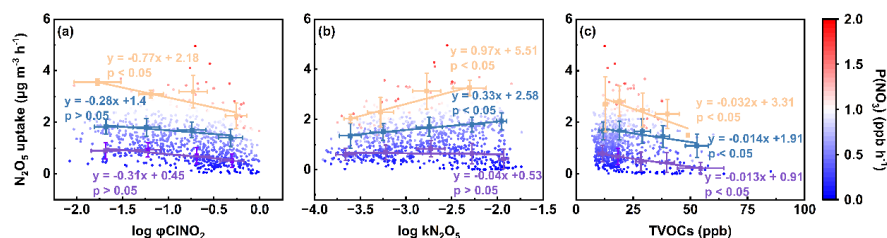


**Figure 5.** Relationships between  $\text{N}_2\text{O}_5$  uptake and  $\phi\text{CINO}_2$  (a),  $\text{kN}_2\text{O}_5$  (b), and TVOCs (c) colored by  $\text{P}(\text{NO}_3)$ . Linear fit curves in purple, blue and orange represent the fitting results for  $\text{P}(\text{NO}_3)$  in the ranges of  $0\text{--}0.5\text{ ppb h}^{-1}$ ,  $0.5\text{--}1.0\text{ ppb h}^{-1}$  and  $> 1.0\text{ ppb h}^{-1}$ , respectively.

### 3.4 Optimal Mitigation Strategies of $\text{pNO}_3^-$ under High $\text{N}_2\text{O}_5$ Uptake.

The above results revealed that  $\text{pNO}_3^-$  formation through both the daytime  $\text{OH} + \text{NO}_2$  reaction and nocturnal heterogeneous  $\text{N}_2\text{O}_5$  uptake was closely linked to VOCs- $\text{NO}_x$ - $\text{O}_3$  chemistry (Yang et al., 2022). Using a multiphase box model, we systematically examined the responses of both  $\text{pNO}_3^-$  and  $\text{O}_3$  to varying  $\text{NO}_x$  and VOC emission scenarios. **Figure 6a** shows  $\text{pNO}_3^-$  formation located in the transition regime of VOCs and  $\text{NO}_x$ . The formation rate of  $\text{pNO}_3^-$  ( $\text{PNO}_3^-$ ) decreased with the reductions of VOCs and  $\text{NO}_x$ , and this trend became more pronounced under aggressive  $\text{NO}_x$  reduction scenarios (**Figure 6c-d**). **Figure S10a-b** reveal that the mean response strength (RS, as defined in Methods) of  $\text{PNO}_3^-$  to  $\text{NO}_x$  was 0.75, higher than that for VOCs ( $\text{RS} = 0.29$ ), suggesting that  $\text{NO}_x$  reduction had a greater potential for  $\text{pNO}_3^-$  mitigation compared to VOCs control. However,  $\text{NO}_x$  and VOCs reductions exerted different impacts on  $\text{O}_3$  formation rate ( $\text{PO}_3$ ). In our study area,  $\text{PO}_3$  located in the VOC-limited regime (**Figure 6b**). We found that  $\text{PO}_3$  declined with VOCs reduction but increased with  $\text{NO}_x$  reduction until  $\text{NO}_x$  dropped below 20% of the base (**Figure 5c-d**). Moreover, detailed results distinguishing daytime and nighttime major formation pathways of  $\text{pNO}_3^-$  are presented in **Figure 6e-f** and **Fig. S10c-d**. For VOC reduction scenarios, both the  $\text{OH} + \text{NO}_2$  reaction and  $\text{N}_2\text{O}_5$  uptake pathways showed declining nitrate formation rates, with comparable RS of 0.11 and 0.18, respectively. This occurs because reduced VOCs concentrations decrease  $\text{OH}$  radical and  $\text{O}_3$  concentrations, thereby suppressing  $\text{pNO}_3^-$  formation via both pathways. In contrast,  $\text{NO}_x$  reduction yielded more complex behavior. The  $\text{OH} + \text{NO}_2$  reaction rates remained nearly constant until  $\text{NO}_x$  dropped to 60% of the base. This stability arises because  $\text{NO}_x$  reduction diminishes the  $\text{NO}$  titration effect on  $\text{O}_3$ , thereby increasing  $\text{OH}$  radicals through  $\text{O}_3$  photolysis.



348 The competing effects of NO<sub>x</sub> reduction and OH enhancement led to an initial plateau in the OH + NO<sub>2</sub>  
 349 reaction rate before its eventual decline. Differently, the N<sub>2</sub>O<sub>5</sub> uptake rate decreased consistently and  
 350 significantly with NO<sub>x</sub> abatement, exhibiting a high mean RS value of 0.61. This phenomenon was  
 351 closely associated with the NO<sub>2</sub>-limited regime of N<sub>2</sub>O<sub>5</sub> uptake in the study area. As shown in **Figure**  
 352 **S11**, the variation trends of pNO<sub>3</sub><sup>-</sup>, P(O<sub>3</sub>), OH + NO<sub>2</sub>, and N<sub>2</sub>O<sub>5</sub> uptake were consistent across all  
 353 VOCs/NO<sub>x</sub> combinations, indicating that the results robustly reflect the response mechanisms to  
 354 precursor emission changes.

355 As mentioned above, VOC reduction proved effective yet limited in mitigating both pNO<sub>3</sub><sup>-</sup> and O<sub>3</sub>,  
 356 the effectiveness of NO<sub>x</sub> reduction exhibited significant regional and temporal variations. In China's  
 357 megacities, including PRD, YRD, and BTH regions, pNO<sub>3</sub><sup>-</sup> initially increased and then decreased in  
 358 response to the reduction of NO<sub>x</sub> emissions (Li et al., 2021; Zhang et al., 2023b; Yang et al., 2022). Under  
 359 high-NO<sub>x</sub> conditions, mild NO<sub>x</sub> reduction would raise daytime OH and O<sub>3</sub> concentrations (Zhang et al.,  
 360 2023b), rendering OH (rather than NO<sub>x</sub>) the limiting factor for the OH + NO<sub>2</sub> reaction, which  
 361 consequently enhanced daytime pNO<sub>3</sub><sup>-</sup> formation. Additionally, as the season most susceptible to PM  
 362 pollution, wintertime N<sub>2</sub>O<sub>5</sub> formation in these regions was in an O<sub>3</sub>-limited or transition regime (Ma et  
 363 al., 2023), wherein the elevated daytime O<sub>3</sub> significantly enhanced NO<sub>3</sub> radical generation, thereby  
 364 promoting nocturnal N<sub>2</sub>O<sub>5</sub> uptake and subsequent pNO<sub>3</sub><sup>-</sup> formation. Conversely, in NO<sub>2</sub>-limited regions  
 365 (e.g., southeastern China), NO<sub>x</sub> reduction showed limited impact on daytime pNO<sub>3</sub><sup>-</sup> formation via the  
 366 OH + NO<sub>2</sub> pathway but effectively suppressed nighttime pNO<sub>3</sub><sup>-</sup> formation via N<sub>2</sub>O<sub>5</sub> uptake. This  
 367 approach concurrently reduced ClNO<sub>2</sub> formation from N<sub>2</sub>O<sub>5</sub> heterogeneous processes, consequently  
 368 diminishing next-day Cl radical generation and its positive feedback on O<sub>3</sub> formation. Considering NO<sub>x</sub>  
 369 reduction during the daytime would cause O<sub>3</sub> formation and only a slight reduction in pNO<sub>3</sub><sup>-</sup>, it is  
 370 preferable to regulate NO<sub>x</sub> at night (18:00–06:00 the next day). Our findings demonstrate that in NO<sub>2</sub>-  
 371 limited regions, targeted NO<sub>x</sub> reduction can synergistically decrease both pNO<sub>3</sub><sup>-</sup> and O<sub>3</sub> concentrations,  
 372 highlighting the critical need to tailor mitigation strategies for different regions.

373



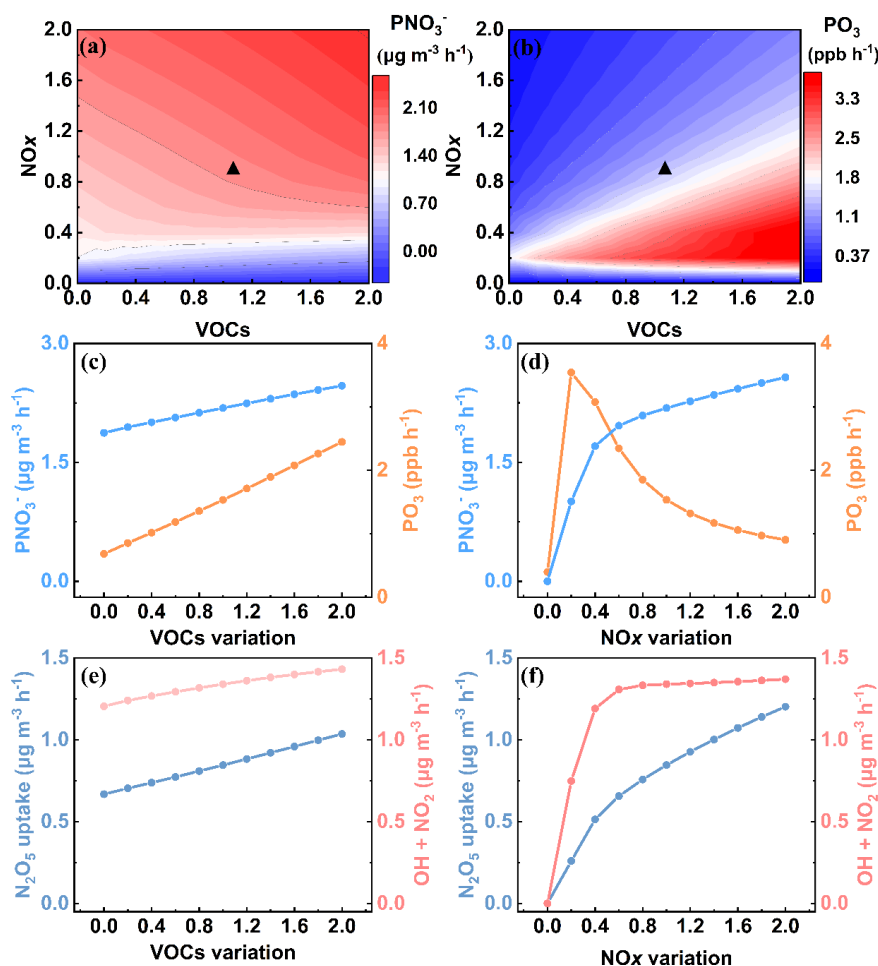


**Figure 6.** Results of multi-scenario simulations obtained from an observation-constrained box model. Isopleths of simulated  $\text{pNO}_3^-$  (a) and  $\text{PO}_3$  (b) with normalized VOCs and  $\text{NO}_x$ . Simulated mean formation rates of  $\text{pNO}_3^-$  and  $\text{O}_3$  (c, d), as well as  $\text{pNO}_3^-$  formation rates via  $\text{N}_2\text{O}_5$  uptake and  $\text{OH} + \text{NO}_2$  (e, f) with normalized VOCs and  $\text{NO}_x$ . The  $\text{pNO}_3^-$  and  $\text{PO}_3$  denote the formation rates of  $\text{pNO}_3^-$  and  $\text{O}_3$ , respectively. The simulated results are daily mean values, and the black triangle indicates the base case for winter 2022. In addition, the results in panel c-f were obtained by maintaining either  $\text{NO}_x$  or VOCs at the base emission rate while varying the other.

## Conclusions and Implications

Our observations revealed a bimodal diurnal pattern of  $\text{pNO}_3^-$  in winter in urban Xiamen. The co-



occurrence of elevated nighttime  $\text{pNO}_3^-$  levels with increased  $\text{N}_2\text{O}_5$  implied a significant contribution of  $\text{N}_2\text{O}_5$  uptake to  $\text{pNO}_3^-$  formation. Quantitative model analysis showed that  $\text{N}_2\text{O}_5$  uptake contributed 51.2% of the total daily  $\text{pNO}_3^-$ , which was comparable to the  $\text{OH} + \text{NO}_2$  reaction. This high contribution of  $\text{N}_2\text{O}_5$  uptake is not commonly observed across Chinese cities. Comparative analysis among different cities suggests that this phenomenon is likely associated with  $\text{NO}_2$ -limited conditions for  $\text{N}_2\text{O}_5$  uptake in our study area. Machine learning results further demonstrated that  $\text{N}_2\text{O}_5$  uptake was driven by nocturnal atmospheric oxidation capacity ( $\text{PNO}_3$ ) rather than heterogeneous uptake conditions. The underlying mechanism is that the weakened  $\text{NO}_x$  titration effects lead to nighttime  $\text{O}_3$  accumulation, which promotes  $\text{NO}_3$  radical generation and consequently enhances  $\text{N}_2\text{O}_5$  and  $\text{pNO}_3^-$  formation. The joint response of  $\text{pNO}_3^-$  and  $\text{O}_3$  to various  $\text{NO}_x$  and VOCs emission scenarios indicated that  $\text{pNO}_3^-$  was more sensitive to  $\text{NO}_x$  reduction than to VOCs reduction. However, mild  $\text{NO}_x$  reduction showed limited effectiveness in reducing daytime  $\text{pNO}_3^-$  while simultaneously increasing  $\text{O}_3$  concentrations. Our findings suggest that  $\text{NO}_x$  reduction is more effective when implemented during nighttime, particularly in regions where  $\text{N}_2\text{O}_5$  formation is  $\text{NO}_2$ -limited. This approach can effectively control  $\text{pNO}_3^-$  formation by suppressing nocturnal  $\text{NO}_3$  radical generation and consequently inhibiting  $\text{N}_2\text{O}_5$  uptake, while simultaneously alleviate  $\text{O}_3$  pollution by reducing  $\text{ClNO}_2$  formation. With continuous  $\text{NO}_x$  and VOCs emission reductions and renewable energy adoption in China, urban areas are transitioning from  $\text{NO}_x$ -saturated to  $\text{NO}_x$ -limited conditions, potentially increasing the importance of  $\text{N}_2\text{O}_5$  uptake. In this context, comprehensive assessment of  $\text{NO}_x$  reduction impacts on urban  $\text{pNO}_3^-$  and  $\text{O}_3$  pollution, along with the development of region-specific mitigation strategies, becomes critically important.

#### **Data Availability**

The dataset for this paper can be accessed at <https://doi.org/10.6084/m9.figshare.29670629> (Lin et al., 2025).

#### **Code Availability**

Data analysis methods are available from the authors upon request.

#### **Acknowledgements**

This work was funded by the National Natural Science Foundation of China (U22A20578), the guiding



project of seizing the commanding heights of “self-purifying city” (IUE-CERAE-202402), the National Key Research and Development Program (2022YFC3700304), STS Plan Supporting Project of the Chinese Academy of Sciences in Fujian Province (2023T3013), and Xiamen Atmospheric Environment Observation and Research Station of Fujian Province.

419

#### 420 **Author Contribution**

421 Z.L. contributed to the methodology, data curation, software, analysis and writing of the original draft.  
 422 L.X. and J.C. contributed to the conceptualization, investigation, data curation, reviewing and editing the  
 423 text, supervision, and funding acquisition. C.Y., X.J., K.Z., F.Z., G.C., L.L., C.Y., Y.C., and Z.C. provided  
 424 useful advice and revised the manuscript.

425

#### 426 **Competing interests**

427 The authors declare no competing interests.

428

#### 429 **REFERENCES**

- 430 Atkinson, R. and Arey, J.: Atmospheric degradation of volatile organic compounds, Chemical Reviews.  
 431 103, 4605-4638, <https://doi.org/10.1021/cr0206420>, 2003.  
 432 Brown, S. S. and Stutz, J.: Nighttime radical observations and chemistry, Chemical Society Reviews. 41,  
 433 6405-6447, <https://doi.org/10.1039/c2cs35181a>, 2012.  
 434 Brown, S. S., Stark, H., and Ravishankara, A. R.: Applicability of the steady state approximation to the  
 435 interpretation of atmospheric observations of NO<sub>3</sub> and N<sub>2</sub>O<sub>5</sub> -: art. no. 4539, Journal of Geophysical  
 436 Research-Atmospheres. 108, <https://doi.org/10.1029/2003jd003407>, 2003.  
 437 Chen, X., Ma, W., Zheng, F. X., Wang, Z. C., Hua, C. J., Li, Y. R., Wu, J., Li, B. D., Jiang, J. K., Yan, C.,  
 438 Petäjä, T., Bianchi, F., Kerminen, V. M., Worsnop, D. R., Liu, Y. C., Xia, M., and Kulmala, M.: Identifying  
 439 Driving Factors of Atmospheric N<sub>2</sub>O<sub>5</sub> with Machine Learning, Environmental Science & Technology.  
 440 <https://doi.org/10.1021/acs.est.4c00651>, 2024.  
 441 Chen, X. R., Wang, H. C., and Lu, K. D.: Interpretation of NO<sub>3</sub>-N<sub>2</sub>O<sub>5</sub> observation via steady state in high-  
 442 aerosol air mass: the impact of equilibrium coefficient in ambient conditions, Atmospheric Chemistry  
 443 and Physics. 22, 3525-3533, <https://doi.org/10.5194/acp-22-3525-2022>, 2022.  
 444 Chen, X. R., Wang, H. C., Lu, K. D., Li, C. M., Zhai, T. Y., Tan, Z. F., Ma, X. F., Yang, X. P., Liu, Y. H.,  
 445 Chen, S. Y., Dong, H. B., Li, X., Wu, Z. J., Hu, M., Zeng, L. M., and Zhang, Y. H.: Field Determination  
 446 of Nitrate Formation Pathway in Winter Beijing, Environmental Science & Technology. 54, 9243-9253,  
 447 <https://doi.org/10.1021/acs.est.0c00972>, 2020.  
 448 Cheng, C. L., Yang, S. X., Yuan, B., Pei, C. L., Zhou, Z. H., Mao, L. Y., Liu, S. L., Chen, D. Y., Cheng,  
 449 X. Y., Li, M., Shao, M., and Zhou, Z.: The significant contribution of nitrate to a severe haze event in the  
 450 winter of Guangzhou, China, Science of the Total Environment. 909,  
 451 <https://doi.org/10.1016/j.scitotenv.2023.168582>, 2024.



- 452 Ehhalt, D. H. and Rohrer, F.: Dependence of the OH concentration on solar UV, *Journal of Geophysical*  
 453 *Research-Atmospheres*. 105, 3565-3571, <https://doi.org/10.1029/1999jd901070>, 2000.
- 454 Fu, X. X., Wang, X. M., Liu, T. Y., He, Q. F., Zhang, Z., Zhang, Y. L., Song, W., Dai, Q. W., Chen, S.,  
 455 and Dong, F. Q.: Secondary inorganic aerosols and aerosol acidity at different PM<sub>2.5</sub> pollution levels  
 456 during winter haze episodes in the Sichuan Basin, China, *Science of the Total Environment*. 918,  
 457 <https://doi.org/10.1016/j.scitotenv.2024.170512>, 2024.
- 458 Gui, K., Che, H. Z., Zeng, Z. L., Wang, Y. Q., Zhai, S. X., Wang, Z. M., Luo, M., Zhang, L., Liao, T. T.,  
 459 Zhao, H. J., Li, L., Zheng, Y., and Zhang, X. Y.: Construction of a virtual PM<sub>2.5</sub> observation network in  
 460 China based on high-density surface meteorological observations using the Extreme Gradient Boosting  
 461 model, *Environment International*. 141, <https://doi.org/10.1016/j.envint.2020.105801>, 2020.
- 462 Hersbach, H., Bell, B., Berrisford, P., Hirahara, S., Horányi, A., Muñoz-Sabater, J., Nicolas, J., Peubey,  
 463 C., Radu, R., Schepers, D., Simmons, A., Soci, C., Abdalla, S., Abellan, X., Balsamo, G., Bechtold, P.,  
 464 Biavati, G., Bidlot, J., Bonavita, M., De Chiara, G., Dahlgren, P., Dee, D., Diamantakis, M., Dragani, R.,  
 465 Flemming, J., Forbes, R., Fuentes, M., Geer, A., Haimberger, L., Healy, S., Hogan, R. J., Hólm, E.,  
 466 Janisková, M., Keeley, S., Laloyaux, P., Lopez, P., Lupu, C., Radnoti, G., de Rosnay, P., Rozum, I.,  
 467 Vamborg, F., Villaume, S., and Thépaut, J. N.: The ERA5 global reanalysis, *Quarterly Journal of the*  
 468 *Royal Meteorological Society*. 146, 1999-2049, <https://doi.org/10.1002/qj.3803>, 2020.
- 469 Huang, X., Ding, A. J., Wang, Z. L., Ding, K., Gao, J., Chai, F. H., and Fu, C. B.: Amplified transboundary  
 470 transport of haze by aerosol-boundary layer interaction in China, *Nature Geoscience*. 13, 428-+,  
 471 <https://doi.org/10.1038/s41561-020-0583-4>, 2020.
- 472 Jenkin, M. E., Young, J. C., and Rickard, A. R.: The MCM v3.3.1 degradation scheme for isoprene,  
 473 *Atmospheric Chemistry and Physics*. 15, 11433-11459, <https://doi.org/10.5194/acp-15-11433-2015>,  
 474 2015.
- 475 Jia, S. G., Chen, W. H., Zhang, Q., Krishnan, P., Mao, J. Y., Zhong, B. Q., Huang, M. J., Fan, Q., Zhang,  
 476 J. P., Chang, M., Yang, L. M., and Wang, X. M.: A quantitative analysis of the driving factors affecting  
 477 seasonal variation of aerosol pH in Guangzhou, China, *Science of the Total Environment*. 725,  
 478 <https://doi.org/10.1016/j.scitotenv.2020.138228>, 2020.
- 479 Lelieveld, J., Evans, J. S., Fnais, M., Giannadaki, D., and Pozzer, A.: The contribution of outdoor air  
 480 pollution sources to premature mortality on a global scale, *Nature*. 525, 367-+,  
 481 <https://doi.org/10.1038/nature15371>, 2015.
- 482 Li, F. B., Huang, D. D., Nie, W., Tham, Y. J., Lou, S. R., Li, Y. Y., Tian, L. H., Liu, Y. L., Zhou, M., Wang,  
 483 H. C., Qiao, L. P., Wang, H. L., Wang, Z., Huang, C., and Li, Y. J.: Observation of nitrogen oxide-  
 484 influenced chlorine chemistry and source analysis of Cl<sub>2</sub> in the Yangtze River Delta, China, *Atmospheric*  
 485 *Environment*. 306, <https://doi.org/10.1016/j.atmosenv.2023.119829>, 2023.
- 486 Li, M. M., Zhang, Z. H., Yao, Q., Wang, T. J., Xie, M., Li, S., Zhuang, B. L., and Han, Y.: Nonlinear  
 487 responses of particulate nitrate to NO<sub>x</sub> emission controls in the megalopolises of China, *Atmospheric*  
 488 *Chemistry and Physics*. 21, 15135-15152, <https://doi.org/10.5194/acp-21-15135-2021>, 2021.
- 489 Lin, Z., Xu, L., Yang, C., Chen, G., Ji, X., Li, L., Zhang, K., Hong, Y., Li, M., Fan, X., Hu, B., Zhang, F.,  
 490 and Chen, J.: Trends of peroxyacetyl nitrate and its impact on ozone over 2018–2022 in urban atmosphere,  
 491 *npj Climate and Atmospheric Science*. 7, 192, <https://doi.org/10.1038/s41612-024-00746-7>, 2024.
- 492 Lin, Ziyi (2025). Data availability about the measurement report titled "Measurement report: High  
 493 contribution of N<sub>2</sub>O<sub>5</sub> uptake to particulate nitrate formation in NO<sub>2</sub>-limited urban areas". figshare.  
 494 Dataset. <https://doi.org/10.6084/m9.figshare.29670629.v1>
- 495 Liu, M. X., Huang, X., Song, Y., Tang, J., Cao, J. J., Zhang, X. Y., Zhang, Q., Wang, S. X., Xu, T. T.,



496 Kang, L., Cai, X. H., Zhang, H. S., Yang, F. M., Wang, H. B., Yu, J. Z., Lau, A. K. H., He, L. Y., Huang,  
 497 X. F., Duan, L., Ding, A. J., Xue, L. K., Gao, J., Liu, B., and Zhu, T.: Ammonia emission control in China  
 498 would mitigate haze pollution and nitrogen deposition, but worsen acid rain, *Proceedings of the National*  
 499 *Academy of Sciences of the United States of America*. 116, 7760-7765,  
 500 <https://doi.org/10.1073/pnas.1814880116>, 2019.

501 Liu, T. T., Hong, Y. W., Li, M. R., Xu, L. L., Chen, J. S., Bian, Y. H., Yang, C., Dan, Y. B., Zhang, Y. N.,  
 502 Xue, L. K., Zhao, M., Huang, Z., and Wang, H.: Atmospheric oxidation capacity and ozone pollution  
 503 mechanism in a coastal city of southeastern China: analysis of a typical photochemical episode by an  
 504 observation-based model, *Atmospheric Chemistry and Physics*. 22, 2173-2190,  
 505 <https://doi.org/10.5194/acp-22-2173-2022>, 2022.

506 Liu, Y., Wang, Y., Ma, P., Ma, Y., Pan, Y., Ma, W., Li, S., Liu, P., Liao, Z., Liu, Z., Chu, B., Ma, Q., Quan,  
 507 J., and He, H.: Formation of Nitrate in the Residual Layer of Beijing: Pathways Evaluation and  
 508 Contributions to the Ground Level, *Environmental Science & Technology*. 59, 9699-9708,  
 509 <https://doi.org/10.1021/acs.est.5c02981>, 2025.

510 Ma, P. K., Quan, J. N., Dou, Y. J., Pan, Y. B., Liao, Z. H., Cheng, Z. G., Jia, X. C., Wang, Q. Q., Zhan, J.  
 511 L., Ma, W., Zheng, F. X., Wang, Y. Z., Zhang, Y. S., Hua, C. J., Yan, C., Kulmala, M., Liu, Y. A., Huang,  
 512 X., Yuan, B., Brown, S. S., and Liu, Y. C.: Regime-Dependence of Nocturnal Nitrate Formation via N<sub>2</sub>O<sub>5</sub>  
 513 Hydrolysis and Its Implication for Mitigating Nitrate Pollution, *Geophysical Research Letters*. 50,  
 514 <https://doi.org/10.1029/2023gl106183>, 2023.

515 Mao, J. Y., Yan, F. H., Zheng, L. M., You, Y. C., Wang, W. W., Jia, S. G., Liao, W. H., Wang, X. M., and  
 516 Chen, W. H.: Ozone control strategies for local formation- and regional transport-dominant scenarios in  
 517 a manufacturing city in southern China, *Science of the Total Environment*. 813,  
 518 <https://doi.org/10.1016/j.scitotenv.2021.151883>, 2022.

519 McDuffie, E. E., Womack, C. C., Fibiger, D. L., Dube, W. P., Franchin, A., Middlebrook, A. M.,  
 520 Goldberger, L., Lee, B., Thornton, J. A., Moravek, A., Murphy, J. G., Baasandorj, M., and Brown, S. S.:  
 521 On the contribution of nocturnal heterogeneous reactive nitrogen chemistry to particulate matter  
 522 formation during wintertime pollution events in Northern Utah, *Atmospheric Chemistry and Physics*. 19,  
 523 9287-9308, <https://doi.org/10.5194/acp-19-9287-2019>, 2019.

524 McDuffie, E. E., Fibiger, D. L., Dubé, W. P., Hilfiker, F. L., Lee, B. H., Jaeglé, L., Guo, H. Y., Weber, R.  
 525 J., Reeves, J. M., Weinheimer, A. J., Schroder, J. C., Campuzano-Jost, P., Jimenez, J. L., Dibb, J. E.,  
 526 Veres, P., Ebben, C., Sparks, T. L., Wooldridge, P. J., Cohen, R. C., Campos, T., Hall, S. R., Ullmann, K.,  
 527 Roberts, J. M., Thornton, J. A., and Brown, S. S.: ClNO<sub>2</sub> Yields From Aircraft Measurements During the  
 528 2015 WINTER Campaign and Critical Evaluation of the Current Parameterization, *Journal of*  
 529 *Geophysical Research-Atmospheres*. 123, 12994-13015, <https://doi.org/10.1029/2018jd029358>, 2018a.

530 McDuffie, E. E., Fibiger, D. L., Dubé, W. P., Lopez-Hilfiker, F., Lee, B. H., Thornton, J. A., Shah, V.,  
 531 Jaeglé, L., Guo, H. Y., Weber, R. J., Reeves, J. M., Weinheimer, A. J., Schroder, J. C., Campuzano-Jost,  
 532 P., Jimenez, J. L., Dibb, J. E., Veres, P., Ebben, C., Sparks, T. L., Wooldridge, P. J., Cohen, R. C.,  
 533 Hornbrook, R. S., Apel, E. C., Campos, T., Hall, S. R., Ullmann, K., and Brown, S. S.: Heterogeneous  
 534 N<sub>2</sub>O<sub>5</sub> Uptake During Winter: Aircraft Measurements During the 2015 WINTER Campaign and Critical  
 535 Evaluation of Current Parameterizations, *Journal of Geophysical Research-Atmospheres*. 123, 4345-  
 536 4372, <https://doi.org/10.1002/2018jd028336>, 2018b.

537 Morgan, W. T., Ouyang, B., Allan, J. D., Aruffo, E., Di Carlo, P., Kennedy, O. J., Lowe, D., Flynn, M. J.,  
 538 Rosenberg, P. D., Williams, P. I., Jones, R., McFiggans, G. B., and Coe, H.: Influence of aerosol chemical  
 539 composition on N<sub>2</sub>O<sub>5</sub> uptake: airborne regional measurements in northwestern Europe, *Atmospheric*



- 540 Chemistry and Physics. 15, 973-990, <https://doi.org/10.5194/acp-15-973-2015>, 2015.
- 541 Niu, Y. B., Zhu, B., He, L. Y., Wang, Z., Lin, X. Y., Tang, M. X., and Huang, X. F.: Fast Nocturnal  
 542 Heterogeneous Chemistry in a Coastal Background Atmosphere and Its Implications for Daytime  
 543 Photochemistry, Journal of Geophysical Research-Atmospheres. 127,  
 544 <https://doi.org/10.1029/2022jd036716>, 2022.
- 545 Requia, W. J., Di, Q., Silvern, R., Kelly, J. T., Koutrakis, P., Mickley, L. J., Sulprizio, M. P., Amini, H.,  
 546 Shi, L. H., and Schwartz, J.: An Ensemble Learning Approach for Estimating High Spatiotemporal  
 547 Resolution of Ground-Level Ozone in the Contiguous United States, Environmental Science &  
 548 Technology. 54, 11037-11047, <https://doi.org/10.1021/acs.est.0c01791>, 2020.
- 549 Seinfeld, J. H.: URBAN AIR-POLLUTION - STATE OF THE SCIENCE, Science. 243, 745-752,  
 550 <https://doi.org/10.1126/science.243.4892.745>, 1989.
- 551 Sun, J. J., Qin, M. M., Xie, X. D., Fu, W. X., Qin, Y., Sheng, L., Li, L., Li, J. Y., Sulaymon, I. D., Jiang,  
 552 L., Huang, L., Yu, X. N., and Hu, J. L.: Seasonal modeling analysis of nitrate formation pathways in  
 553 Yangtze River Delta region, China, Atmospheric Chemistry and Physics. 22, 12629-12646,  
 554 <https://doi.org/10.5194/acp-22-12629-2022>, 2022.
- 555 Thaler, R. D., Mielke, L. H., and Osthoff, H. D.: Quantification of Nitryl Chloride at Part Per Trillion  
 556 Mixing Ratios by Thermal Dissociation Cavity Ring-Down Spectroscopy, Analytical Chemistry. 83,  
 557 2761-2766, <https://doi.org/10.1021/ac200055z>, 2011.
- 558 Tham, Y. J., Wang, Z., Li, Q. Y., Wang, W. H., Wang, X. F., Lu, K. D., Ma, N., Yan, C., Kecorius, S.,  
 559 Wiedensohler, A., Zhang, Y. H., and Wang, T.: Heterogeneous N<sub>2</sub>O<sub>5</sub> uptake coefficient and production  
 560 yield of ClNO<sub>2</sub> in polluted northern China: roles of aerosol water content and chemical composition,  
 561 Atmospheric Chemistry and Physics. 18, 13155-13171, <https://doi.org/10.5194/acp-18-13155-2018>,  
 562 2018.
- 563 Tham, Y. J., Wang, Z., Li, Q. Y., Yun, H., Wang, W. H., Wang, X. F., Xue, L. K., Lu, K. D., Ma, N., Bohn,  
 564 B., Li, X., Kecorius, S., Gröss, J., Shao, M., Wiedensohler, A., Zhang, Y. H., and Wang, T.: Significant  
 565 concentrations of nitryl chloride sustained in the morning: investigations of the causes and impacts on  
 566 ozone production in a polluted region of northern China, Atmospheric Chemistry and Physics. 16, 14959-  
 567 14977, <https://doi.org/10.5194/acp-16-14959-2016>, 2016.
- 568 Wagner, N. L., Riedel, T. P., Young, C. J., Bahreini, R., Brock, C. A., Dubé, W. P., Kim, S., Middlebrook,  
 569 A. M., Öztürk, F., Roberts, J. M., Russo, R., Sive, B., Swarthout, R., Thornton, J. A., VandenBoer, T. C.,  
 570 Zhou, Y., and Brown, S. S.: N<sub>2</sub>O<sub>5</sub> uptake coefficients and nocturnal NO<sub>2</sub> removal rates determined from  
 571 ambient wintertime measurements, Journal of Geophysical Research-Atmospheres. 118, 9331-9350,  
 572 <https://doi.org/10.1002/jgrd.50653>, 2013.
- 573 Wang, H. C., Lu, K. D., Chen, S. Y., Li, X., Zeng, L. M., Hu, M., and Zhang, Y. H.: Characterizing nitrate  
 574 radical budget trends in Beijing during 2013-2019, Science of the Total Environment. 795,  
 575 <https://doi.org/10.1016/j.scitotenv.2021.148869>, 2021.
- 576 Wang, H. C., Wang, H. L., Lu, X., Lu, K. D., Zhang, L., Tham, Y. J., Shi, Z. B., Aikin, K., Fan, S. J.,  
 577 Brown, S. S., and Zhang, Y. H.: Increased night-time oxidation over China despite widespread decrease  
 578 across the globe, Nature Geoscience. 16, 217-+, <https://doi.org/10.1038/s41561-022-01122-x>, 2023a.
- 579 Wang, H. C., Peng, C., Wang, X., Lou, S. R., Lu, K. D., Gan, G. C., Jia, X. H., Chen, X. R., Chen, J.,  
 580 Wang, H. L., Fan, S. J., Wang, X. M., and Tang, M. J.: N<sub>2</sub>O<sub>5</sub> uptake onto saline mineral dust: a potential  
 581 missing source of tropospheric ClNO<sub>2</sub> in inland China, Atmospheric Chemistry and Physics. 22, 1845-  
 582 1859, <https://doi.org/10.5194/acp-22-1845-2022>, 2022a.
- 583 Wang, H. C., Lu, K. D., Guo, S., Wu, Z. J., Shang, D. J., Tan, Z. F., Wang, Y. J., Le Breton, M., Lou, S.



- 584 R., Tang, M. J., Wu, Y. S., Zhu, W. F., Zheng, J., Zeng, L. M., Hallquist, M., Hu, M., and Zhang, Y. H.:  
 585 Efficient  $\text{N}_2\text{O}_5$  uptake and  $\text{NO}_3$  oxidation in the outflow of urban Beijing, *Atmospheric Chemistry and*  
 586 *Physics*. 18, 9705-9721, <https://doi.org/10.5194/acp-18-9705-2018>, 2018.
- 587 Wang, H. C., Lu, K. D., Chen, X. R., Zhu, Q. D., Chen, Q., Guo, S., Jiang, M. Q., Li, X., Shang, D. J.,  
 588 Tan, Z. F., Wu, Y. S., Wu, Z. J., Zou, Q., Zheng, Y., Zeng, L. M., Zhu, T., Hu, M., and Zhang, Y. H.: High  
 589  $\text{N}_2\text{O}_5$  Concentrations Observed in Urban Beijing: Implications of a Large Nitrate Formation Pathway,  
 590 *Environmental Science & Technology Letters*. 4, 416-420, <https://doi.org/10.1021/acs.estlett.7b00341>,  
 591 2017.
- 592 Wang, H. C., Yuan, B., Zheng, E., Zhang, X. X., Wang, J., Lu, K. D., Ye, C. S., Yang, L., Huang, S., Hu,  
 593 W. W., Yang, S. X., Peng, Y. W., Qi, J. P., Wang, S. H., He, X. J., Chen, Y. B., Li, T. G., Wang, W. J.,  
 594 Huangfu, Y. B., Li, X. B., Cai, M. F., Wang, X. M., and Shao, M.: Formation and impacts of nitryl chloride  
 595 in Pearl River Delta, *Atmospheric Chemistry and Physics*. 22, 14837-14858, [https://doi.org/10.5194/acp-](https://doi.org/10.5194/acp-22-14837-2022)  
 596 [22-14837-2022](https://doi.org/10.5194/acp-22-14837-2022), 2022b.
- 597 Wang, W. J., Li, X., Cheng, Y. F., Parrish, D. D., Ni, R. J., Tan, Z. F., Liu, Y., Lu, S. H., Wu, Y. S., Chen,  
 598 S. Y., Lu, K. D., Hu, M., Zeng, L. M., Shao, M., Huang, C., Tian, X. D., Leung, K. M., Chen, L. F., Fan,  
 599 M., Zhang, Q., Rohrer, F., Wahner, A., Pöschl, U., Su, H., and Zhang, Y. H.: Ozone pollution mitigation  
 600 strategy informed by long-term trends of atmospheric oxidation capacity, *Nature Geoscience*. 16, 1080-  
 601 1081, <https://doi.org/10.1038/s41561-023-01334-9>, 2023b.
- 602 Wang, Y. H., Gao, W. K., Wang, S., Song, T., Gong, Z. Y., Ji, D. S., Wang, L. L., Liu, Z. R., Tang, G. Q.,  
 603 Huo, Y. F., Tian, S. L., Li, J. Y., Li, M. G., Yang, Y., Chu, B. W., Petäjä, T., Kerminen, V. M., He, H., Hao,  
 604 J. M., Kulmala, M., Wang, Y. S., and Zhang, Y. H.: Contrasting trends of  $\text{PM}_{2.5}$  and surface-ozone  
 605 concentrations in China from 2013 to 2017, *National Science Review*. 7, 1331-1339,  
 606 <https://doi.org/10.1093/nsr/nwaa032>, 2020.
- 607 Wang, Y. R., Yang, X. Y., Wu, K., Mei, H., De Smedt, I., Wang, S. G., Fan, J., Lyu, S., and He, C.: Long-  
 608 term trends of ozone and precursors from 2013 to 2020 in a megacity (Chengdu), China: Evidence of  
 609 changing emissions and chemistry, *Atmospheric Research*. 278,  
 610 <https://doi.org/10.1016/j.atmosres.2022.106309>, 2022c.
- 611 Wang, Y. T., Zhao, Y., Liu, Y. M., Jiang, Y. Q., Zheng, B., Xing, J., Liu, Y., Wang, S., and Nielsen, C. P.:  
 612 Sustained emission reductions have restrained the ozone pollution over China, *Nature Geoscience*. 16,  
 613 967-+, <https://doi.org/10.1038/s41561-023-01284-2>, 2023c.
- 614 Wen, L., Xue, L. K., Wang, X. F., Xu, C. H., Chen, T. S., Yang, L. X., Wang, T., Zhang, Q. Z., and Wang,  
 615 W. X.: Summertime fine particulate nitrate pollution in the North China Plain: increasing trends,  
 616 formation mechanisms and implications for control policy, *Atmospheric Chemistry and Physics*. 18,  
 617 11261-11275, <https://doi.org/10.5194/acp-18-11261-2018>, 2018.
- 618 Wolfe, G. M., Marvin, M. R., Roberts, S. J., Travis, K. R., and Liao, J.: The Framework for 0-D  
 619 Atmospheric Modeling (F0AM) v3.1, *Geoscientific Model Development*. 9, 3309-3319,  
 620 <https://doi.org/10.5194/gmd-9-3309-2016>, 2016.
- 621 Xie, X. D., Hu, J. L., Qin, M. M., Guo, S., Hu, M., Wang, H. L., Lou, S. R., Li, J. Y., Sun, J. J., Li, X.,  
 622 Sheng, L., Zhu, J. L., Chen, G. Y., Yin, J. J., Fu, W. X., Huang, C., and Zhang, Y. H.: Modeling particulate  
 623 nitrate in China: Current findings and future directions, *Environment International*. 166,  
 624 <https://doi.org/10.1016/j.envint.2022.107369>, 2022.
- 625 Xing, J., Ding, D., Wang, S. X., Zhao, B., Jang, C., Wu, W. J., Zhang, F. F., Zhu, Y., and Hao, J. M.:  
 626 Quantification of the enhanced effectiveness of  $\text{NO}_x$  control from simultaneous reductions of VOC and  
 627  $\text{NH}_3$  for reducing air pollution in the Beijing-Tianjin-Hebei region, China, *Atmospheric Chemistry and*





- 628 Physics. 18, 7799-7814, <https://doi.org/10.5194/acp-18-7799-2018>, 2018.
- 629 Yan, C., Tham, Y. J., Nie, W., Xia, M., Wang, H. C., Guo, Y. S., Ma, W., Zhan, J. L., Hua, C. J., Li, Y. Y.,  
 630 Deng, C. J., Li, Y. R., Zheng, F. X., Chen, X., Li, Q. Y., Zhang, G., Mahajan, A. S., Cuevas, C. A., Huang,  
 631 D. D., Wang, Z., Sun, Y. L., Saiz-Lopez, A., Bianchi, F., Kerminen, V. M., Worsnop, D. R., Donahue, N.  
 632 M., Jiang, J. K., Liu, Y. C., Ding, A. J., and Kulmala, M.: Increasing contribution of nighttime nitrogen  
 633 chemistry to wintertime haze formation in Beijing observed during COVID-19 lockdowns, *Nature*  
 634 *Geoscience*. 16, 975-+, <https://doi.org/10.1038/s41561-023-01285-1>, 2023.
- 635 Yang, C., Dong, H. S., Chen, Y. P., Xu, L. L., Chen, G. J., Fan, X. L., Wang, Y. H., Tham, Y. J., Lin, Z.  
 636 Y., Li, M. R., Hong, Y. W., and Chen, J. S.: New Insights on the Formation of Nucleation Mode Particles  
 637 in a Coastal City Based on a Machine Learning Approach, *Environmental Science & Technology*. 58,  
 638 1187-1198, <https://doi.org/10.1021/acs.est.3c07042>, 2023.
- 639 Yang, S. X., Yuan, B., Peng, Y. W., Huang, S., Chen, W., Hu, W. W., Pei, C. L., Zhou, J., Parrish, D. D.,  
 640 Wang, W. J., He, X. J., Cheng, C. L., Li, X. B., Yang, X. Y., Song, Y., Wang, H. C., Qi, J. P., Wang, B. L.,  
 641 Wang, C., Wang, C. M., Wang, Z. L., Li, T. G., Zheng, E., Wang, S. H., Wu, C. H., Cai, M. F., Ye, C. S.,  
 642 Song, W., Cheng, P., Chen, D. H., Wang, X. M., Zhang, Z. Y., Wang, X. M., Zheng, J. Y., and Shao, M.:  
 643 The formation and mitigation of nitrate pollution: comparison between urban and suburban environments,  
 644 *Atmospheric Chemistry and Physics*. 22, 4539-4556, <https://doi.org/10.5194/acp-22-4539-2022>, 2022.
- 645 Yu, C., Wang, Z., Xia, M., Fu, X., Wang, W. H., Tham, Y. J., Chen, T. S., Zheng, P. G., Li, H. Y., Shan,  
 646 Y., Wang, X. F., Xue, L. K., Zhou, Y., Yue, D. L., Ou, Y. B., Gao, J., Lu, K. D., Brown, S. S., Zhang, Y.  
 647 H., and Wang, T.: Heterogeneous N<sub>2</sub>O<sub>5</sub> reactions on atmospheric aerosols at four Chinese sites:  
 648 improving model representation of uptake parameters, *Atmospheric Chemistry and Physics*. 20, 4367-  
 649 4378, <https://doi.org/10.5194/acp-20-4367-2020>, 2020.
- 650 Yun, H., Wang, W. H., Wang, T., Xia, M., Yu, C., Wang, Z., Poon, S. C. N., Yue, D. L., and Zhou, Y.:  
 651 Nitrate formation from heterogeneous uptake of dinitrogen pentoxide during a severe winter haze in  
 652 southern China, *Atmospheric Chemistry and Physics*. 18, 17515-17527, [https://doi.org/10.5194/acp-18-](https://doi.org/10.5194/acp-18-17515-2018)  
 653 [17515-2018](https://doi.org/10.5194/acp-18-17515-2018), 2018.
- 654 Zhai, S. X., Jacob, D. J., Wang, X., Liu, Z. R., Wen, T. X., Shah, V., Li, K., Moch, J. M., Bates, K. H.,  
 655 Song, S. J., Shen, L., Zhang, Y. Z., Luo, G., Yu, F. Q., Sun, Y. L., Wang, L. T., Qi, M. Y., Tao, J., Gui, K.,  
 656 Xu, H. H., Zhang, Q., Zhao, T. L., Wang, Y. S., Lee, H. C., Choi, H., and Liao, H.: Control of particulate  
 657 nitrate air pollution in China, *Nature Geoscience*. 14, 389-+, [https://doi.org/10.1038/s41561-021-00726-](https://doi.org/10.1038/s41561-021-00726-z)  
 658 [z](https://doi.org/10.1038/s41561-021-00726-z), 2021.
- 659 Zhai, T. Y., Lu, K. D., Wang, H. C., Lou, S. R., Chen, X. R., Hu, R. Z., and Zhang, Y. H.: Elucidate the  
 660 formation mechanism of particulate nitrate based on direct radical observations in the Yangtze River  
 661 Delta summer 2019, *Atmospheric Chemistry and Physics*. 23, 2379-2391, [https://doi.org/10.5194/acp-](https://doi.org/10.5194/acp-23-2379-2023)  
 662 [23-2379-2023](https://doi.org/10.5194/acp-23-2379-2023), 2023.
- 663 Zhang, R., Han, Y. H., Shi, A. J., Sun, X. S., Yan, X., Huang, Y. H., and Wang, Y.: Characteristics of  
 664 ambient ammonia and its effects on particulate ammonium in winter of urban Beijing, China,  
 665 *Environmental Science and Pollution Research*. 28, 62828-62838, [https://doi.org/10.1007/s11356-021-](https://doi.org/10.1007/s11356-021-14108-w)  
 666 [14108-w](https://doi.org/10.1007/s11356-021-14108-w), 2021.
- 667 Zhang, X., Ma, Q., Chu, W. H., Ning, M., Liu, X. Q., Xiao, F. J., Cai, N. N., Wu, Z. J., and Yan, G.:  
 668 Identify the key emission sources for mitigating ozone pollution: A case study of urban area in the  
 669 Yangtze River Delta region, China, *Science of the Total Environment*. 892,  
 670 <https://doi.org/10.1016/j.scitotenv.2023.164703>, 2023a.
- 671 Zhang, Y., Lei, R., Cui, S., Wang, H., Chen, M., and Ge, X.: Spatiotemporal trends and impact factors of





672 PM<sub>2.5</sub> and O<sub>3</sub> pollution in major cities in China during 2015-2020, Chinese Science Bulletin. 67, 2029-  
 673 2042, 2022.

674 Zhang, Y. N., Wang, H. L., Huang, L. B., Qiao, L. P., Zhou, M., Mu, J. S., Wu, C., Zhu, Y. J., Shen, H.  
 675 Q., Huang, C., Wang, G. H., Wang, T., Wang, W. X., and Xue, L. K.: Double-Edged Role of VOCs  
 676 Reduction in Nitrate Formation: Insights from Observations during the China International Import Expo  
 677 2018, Environmental Science & Technology. 57, 15979-15989, <https://doi.org/10.1021/acs.est.3c04629>,  
 678 2023b.

679 Zhao, S. P., Yin, D. Y., Yu, Y., Kang, S. C., Qin, D. H., and Dong, L. X.: PM<sub>2.5</sub> and O<sub>3</sub> pollution during  
 680 2015-2019 over 367 Chinese cities: Spatiotemporal variations, meteorological and topographical impacts,  
 681 Environmental Pollution. 264, <https://doi.org/10.1016/j.envpol.2020.114694>, 2020.

682 Zhao, X. X., Zhao, X. J., Liu, P. F., Chen, D., Zhang, C. L., Xue, C. Y., Liu, J. F., Xu, J., and Mu, Y. J.:  
 683 Transport Pathways of Nitrate Formed from Nocturnal N<sub>2</sub>O<sub>5</sub> Hydrolysis Aloft to the Ground Level in  
 684 Winter North China Plain, Environmental Science & Technology.  
 685 <https://doi.org/10.1021/acs.est.3c00086>, 2023.

686 Zhou, M., Nie, W., Qiao, L. P., Huang, D. D., Zhu, S. H., Lou, S. R., Wang, H. L., Wang, Q., Tao, S. K.,  
 687 Sun, P., Liu, Y. W., Xu, Z., An, J. Y., Yan, R. S., Su, H., Huang, C., Ding, A. J., and Chen, C. H.: Elevated  
 688 Formation of Particulate Nitrate From N<sub>2</sub>O<sub>5</sub> Hydrolysis in the Yangtze River Delta Region From 2011 to  
 689 2019, Geophysical Research Letters. 49, <https://doi.org/10.1029/2021gl097393>, 2022.

690 Zong, Z., Tian, C. G., Sun, Z. Y., Tan, Y., Shi, Y. J., Liu, X. H., Li, J., Fang, Y. T., Chen, Y. J., Ma, Y. H.,  
 691 Gao, H. W., Zhang, G., and Wang, T.: Long-Term Evolution of Particulate Nitrate Pollution in North  
 692 China: Isotopic Evidence From 10 Offshore Cruises in the Bohai Sea From 2014 to 2019, Journal of  
 693 Geophysical Research-Atmospheres. 127, <https://doi.org/10.1029/2022jd036567>, 2022.

694